A&A 642, A74 (2020)
https://doi.org/10.1051/0004-6361/202038512

Astronomy & Astrophysics

The surface of (1) Ceres in visible light as seen by Dawn/VIR*

B. Rousseau[1], M. C. De Sanctis[1], A. Raponi[1], M. Ciarniello[1], E. Ammannito[2], A. Frigeri[1], M. Ferrari[1], S. De Angelis[1], F. C. Carrozzo[1], F. Tosi[1], S. E. Schröder[3], C. A. Raymond[4], and C. T. Russell[5]

[1] Istituto Nazionale di Astrofisica (INAF) – Istituto di Astrofisica e Planetologia Spaziali (IAPS), Via Fosso del Cavaliere, 100, 00133 Rome, Italy
e-mail: batiste.rousseau@inaf.it
[2] Italian Space Agency (ASI), Via del Politecnico, 00133, Rome Italy
[3] Deutsches Zentrum für Luft- und Raumfahrt (DLR), 12489 Berlin, Germany
[4] Jet Propulsion Laboratory, California Institute of Technology, Pasadena, USA
[5] Earth Planetary and Space Sciences, University of California Los Angeles, Los Angeles, CA, USA

Received 27 May 2020 / Accepted 29 July 2020

ABSTRACT

Aims. We study the surface of Ceres at visible wavelengths, as observed by the Visible and InfraRed mapping spectrometer (VIR) onboard the Dawn spacecraft, and analyze the variations of various spectral parameters across the whole surface. We also focus on several noteworthy areas of the surface of this dwarf planet.
Methods. We made use of the newly corrected VIR visible data to build global maps of a calibrated radiance factor at 550 nm, with two color composites and three spectral slopes between 400 and 950 nm. We have made these maps available for the community via the Aladin Desktop software.
Results. Ceres' surface shows diverse spectral behaviors in the visible range. The color composite and the spectral slope between 480 and 800 nm highlight fresh impact craters and young geologic formations of endogenous origin, which appear bluer than the rest of the surface. The steep slope before 465 nm displays very distinct variations and may be a proxy for the absorptions caused by the $O_2^- \longrightarrow Fe_3^+$ or the $2Fe^{3+} \longrightarrow Fe^{2+} + Fe^{4+}$ charge transfers, if the latter are found to be responsible for the drop in this spectral range. We notice several similarities between the spectral slopes and the abundance of phyllosilicates detected in the infrared by the VIR, whereas no correlation can be clearly established with carbonate species. The region of the Dantu impact crater presents a peculiar spectral behavior – especially through the color and the spectral slope before 465 nm – suggesting a change in composition or in the surface physical properties that is not observed elsewhere on Ceres.

Key words. minor planets, asteroids: individual: Ceres – planets and satellites: surfaces – techniques: imaging spectroscopy – methods: data analysis

1. Introduction

The NASA Dawn spacecraft was launched on September 27, 2007, reaching the asteroid Vesta in July 2011 (Russell et al. 2007). The spacecraft then left Vesta in September 2012 and entered orbit around Ceres in March 2015. The study of the dwarf planet Ceres lasted more than three years, up until the end of October 2018.

Dawn was equipped with three instruments to study the surfaces of Vesta and Ceres: a Framing Camera (FC), with one clear filter and seven narrow band-pass filters (Sierks et al. 2011), which provided optical imagery in the visual range at a high spatial resolution (up to 30 m pixel^{-1} during the low-altitude orbit phase at Ceres); a Gamma Ray and Neutron Detector (GRaND), which sampled the elemental composition of the surface at coarser spatial scales (Prettyman et al. 2011); and a Visible InfraRed mapping spectrometer (VIR), a hyperspectral imager combining spectroscopic and imaging capabilities in the visible to infrared wavelengths (De Sanctis et al. 2011). In this work, we focus on Dawn's observations of Ceres at visible wavelengths as measured by the Visible and InfraRed mapping spectrometer (VIR).

The Dawn orbital mission at Ceres was split into different ranges of altitude over the surface (Russell et al. 2007; De Sanctis et al. 2018a). For details on the different phases of the mission, specifically for the visible channel, see Rousseau et al. (2019). This allowed for observations of the surface at moderate and high spatial resolutions, achieving a nearly global mapping and providing an unprecedented view of the surface of Ceres.

Overall, the surface of Ceres is characterized by an almost flat reflectance spectrum in the spectral region below 2.6 μm, with the exception of a broad inflection at about 1.2 μm, possibly due to iron-bearing materials (Rivkin et al. 2011; De Sanctis et al. 2018a). The 2.6–4.2 μm wavelength region is characterized by a broad asymmetric feature, in which several distinct absorptions show up at 2.72, 3.05–3.1, 3.3–3.5, and 3.95 μm. The strongest, a narrow feature centered at 2.72-2.73 μm, is indicative of the structural OH in Mg-bearing phyllosilicates. The other signatures are attributed to carbonates (~3.9 μm) and ammoniated phyllosilicates (~3.06 μm). The spectra show a broad absorption between 3.3–3.6 μm, which may be the result of overlapping bands due to carbonates, ammoniated-phyllosilicates, and organics (Moroz et al. 1998; Beran 2002; Bishop et al. 2008).

The average Ceres spectrum has been interpreted as the result of a mixture of dark material, Mg-phyllosilicates, ammoniated-phyllosilicates and (Mg, Ca)-carbonates (De Sanctis et al. 2015, 2018a). These materials are present everywhere: no large

* The HipS files are available at the CDS via http://alasky.u-strasbg.fr/pub/10.1051_0004-6361_202038512

km-sized areas lacking the above-mentioned species have been observed (Ammannito et al. 2016; Carrozzo et al. 2018). However, changes in the strength of the absorption features have been reported (Ammannito et al. 2016; Carrozzo et al. 2018), indicating variability in the relative abundance of the phyllosilicates and carbonates. Similarly, ammonium-bearing minerals are ubiquitous on the surface of Ceres, even though they show a difference in abundance and in chemical form (De Sanctis et al. 2016; Ammannito et al. 2016). The observed mineralogy requires pervasive and long-standing aqueous alteration (De Sanctis et al. 2016; Ammannito et al. 2016), as also suggested by the spatial uniformity of element abundance measurements of equatorial regolith (Prettyman et al. 2016; Lawrence et al. 2018).

The global map of hydrogen abundance obtained by GRaND indicates the presence of ice buried below the Cerean regolith, which is increasingly abundant moving away from the equator to high latitudes (Prettyman et al. 2016; Lawrence et al. 2018). Indeed, local exposure of water ice has been identified on the surface of Ceres, for example, in the craters Oxo and Juling (Combe et al. 2016, 2019; Raponi et al. 2018). Sodium carbonates were first detected in the crater Occator's bright faculae (De Sanctis et al. 2016) and later identified in many other bright areas (Zambon et al. 2017; Carrozzo et al. 2018). Moreover, regional areas with organic material have also been detected (De Sanctis et al. 2017, 2018b).

So far, the spectral behavior of Ceres' surface at visible wavelengths, as measured by VIR, has not been deeply investigated due to the presence of instrumental artifacts that have only recently been corrected by Rousseau et al. (2019). Taking advantage of this new spectral calibration, in this work, we provide a global analysis of VIR visible spectral properties and provide updated maps of visible reflectance and related spectral parameter maps.

Details about the VIR instrument, the dataset, and the definition of the spectral parameters, along with their mapping are given in Sect. 2. In Sect. 3, we describe the global maps of the spectral parameters. In Sects. 4 and 5 we discuss our results in light of the existing literature, as well as the VIR infrared observations and of the Framing Camera results. Finally, we present our summary in Sect. 6.

2. Data and methods

2.1. The VIR instrument

The VIR instrument is an imaging spectrometer that combines spatial and spectral information. It is made up of two channels, the first working in the visual wavelengths (VIS, 0.25–1.07 μm) and the second in the infrared (IR, 1.02–5.09 μm). The average spectral sampling in the VIS is 1.8 nm band^{-1} and its instantaneous field of view (IFOV) of 250 μrad × 250 μrad. A detailed description of the instrument is provided by De Sanctis et al. (2011). Here, we focus on the visible dataset acquired by VIR at Ceres, but we limit the analysis in the spectral interval between 400 and 950 nm because of low signal conditions combined with calibration residuals outside this range.

2.2. Data correction and processing

The data used in this study correspond to the calibrated version of the VIR observations (LEVEL 1B) available through the Planetary Data System (PDS) online data archive[1]. They are expressed in units of calibrated radiance factor, as described by Carrozzo et al. (2016). Several corrections have been applied over this calibrated version, which are briefly described below.

A multiplicative matrix is applied on the data in order to correct for the odd-even effect, spectral spikes, vertical stripes, and systematic artifacts. This first procedure is described in Carrozzo et al. (2016). The VIR VIS spectra are affected by a positive slope which has been corrected a first time by Carrozzo et al. (2016), using ground-based observations. Here we replaced and refined this correction by means of the following steps: (1) we collected ground observations of Ceres, which are mutually consistent in the spectral range where they overlap (Chapman & Gaffey 1979; Roettger & Buratti 1994; Parker et al. 2002; Bus & Binzel 2002a,b; Lazzaro et al. 2006; Li et al. 2006; Rivkin et al. 2011); (2) then each ground full-disk observation (point n°1) was converted in bidirectional reflectance at standard viewing geometry (incidence angle = 30°, emission angle = 0°, phase angle = 30°) by means of Hapke modeling (Hapke 2012), according to the photometric parameters derived by Ciarniello et al. (2017); (3) based on the ground-based spectra (point n°2), we calculated a smooth average spectrum which covers the whole spectral range of the visible channel of the VIR spectrometer; (4) we collected VIR data at standard viewing geometry (incidence angle = 30°, emission angle = 0°, phase angle = 30°) and we calculated the average spectrum; (5) finally, we calculated the ratio between the average spectrum from ground observations (point n°3) and the average spectrum obtained from VIR data (point n°4). This ratio spectrum is used as a multiplicative correction factor for every single VIR spectrum.

The data were then photometrically corrected, as described by Ciarniello et al. (2017). This allows the variability of the observation geometry to be discarded. Finally, to overcome spurious spectral variations due to the detector temperature, an empirical correction was developed, as detailed in Rousseau et al. (2019), and applied to the data used in this study.

The data investigated in this work were acquired over four different phases of the Dawn mission at Ceres, lasting from late April 2015 to mid-August 2015 (see Table 1 for more details). The dataset is made up of 505 hyperspectral cubes, corresponding to nearly 8 million single observations. It provides an almost complete coverage of Ceres' surface and a high redundancy, particularly in the 50°S–50°N latitude range (see Fig. A.1).

To deal with this large amount of data, we developed an automatic procedure aimed at calculating different spectral parameters of interest for all the observations of each cube contained in a single mission phase. The results are stored in binary FITS tables to facilitate further processing. We did not apply any filters on the observation angles; this allows us to take advantage of the full dataset. The counterpart is a lower quality rendering at high latitudes due to a less accurate photometric correction for more extreme observation angles (Ciarniello et al. 2017). Finally, in each map, we filtered out several cubes that showed too many artifacts (see Sect. 3).

2.3. Spectral parameters

The spectral variability at the surface of Ceres in the 400–950 nm range was studied through several parameters based on the average spectrum as shown in Fig. 1. This spectrum corresponds to the median of the CSH mission phase observations. Due to their spatial distribution, they are representative of the whole Ceres surface (see Fig. A and Rousseau et al. 2019); the resulting spectrum can be considered as a "mean Ceres" and reliable for the spectral parameter definition.

[1] https://sbn.psi.edu/pds/resource/dawn/dwncvirL1.html

Table 1. Mission phases of Dawn at Ceres used in this study.

Mission phase	Start date (mm-dd)	Stop date (mm-dd)	Cubes (used/total)	Resolution (m pix^{-1})
CSR	04-25	05-07	75/75	3400–3500
CTS	05-16	05-22	12/12	1300–1800
CSS	06-05	06-27	230/280	1000–1100
CSH	08-18	10-21	188/196	360–400

Notes. Mission phases are chronologically sorted and we report only the periods during which VIR visible data were acquired. CSR: Ceres Science Rotational Characterization 3; CTS: Ceres Transfer to Survey; CSS: Ceres Science Survey; CSH: Ceres Science High Altitude Mapping Orbit Ceres. These data were all acquired in 2015. In the fourth column, a discrepancy between processed versus available data arises from the occurrence of sky observation or corrupted data. The fifth column provides the approximate minimum and maximum across-track resolutions.

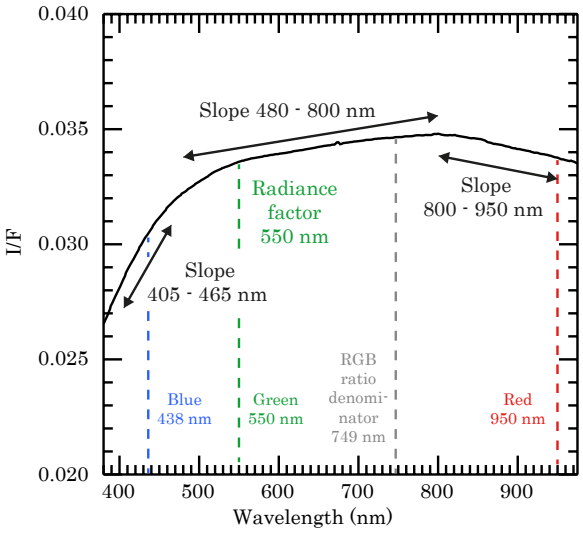

Fig. 1. Median spectrum of Ceres' surface with the spectral parameters used in this study. RGB channels used to build the RGB composite are indicated at the bottom.

The first spectral parameter is the calibrated radiance factor at 550 nm – hereafter called reflectance[2] or $I/F_{550\mathrm{nm}}$. Then, we defined two RGB color composites chosen to closely resemble the ones adopted by Schröder et al. (2017) and Nathues et al. (2016). The first is a simple RGB composite, based on the red, green, and blue colors attributed to the reflectance at 950 nm, 550 nm, and 438 nm, respectively, which shows color and albedo variations. This is both an advantage and an inconvenience since the perception of the albedo variations affects the perception of the colors and vice versa. The second is a RGB ratio – based on the red, green, and blue colors attributed to the reflectance ratios, $I/F_{950\mathrm{nm}}/I/F_{749\mathrm{nm}}$, $I/F_{550\mathrm{nm}}/I/F_{749\mathrm{nm}}$ and $I/F_{438\mathrm{nm}}/I/F_{749\mathrm{nm}}$, respectively. This allows us to get rid of the albedo surface changes and emphasize only the color variations. These two RGB composites are, thus, complementary and useful in the visible spectral domain.

Finally, we used three spectral slopes to enhance the relative spectral variations across the surface. Following the definition adopted by Ciarniello et al. (2015, 2017), each slope, expressed in kÅ^{-1}, is defined by Eq. (1) and written as $S_{\lambda_1-\lambda_2}$, where λ_1 and λ_2 are the wavelengths of each side.

$$S_{\lambda_1-\lambda_2} = \frac{(I/F)_{\lambda_2} - (I/F)_{\lambda_1}}{(I/F)_{\lambda_1} \times (\lambda_2 - \lambda_1)}. \quad (1)$$

The slope, $S_{405-465\mathrm{nm}}$, characterizes the steep drop of reflectance observed before ~480 nm. The second slope, $S_{480-800\mathrm{nm}}$, describes the central part of the spectra, which is mostly flat and between 480 and 800 nm. The third slope is $S_{800-950\mathrm{nm}}$: this range is chosen to characterize the near-IR part of the channel, where a slight negative slope is observed.

2.4. Map projections

The maps presented in Sect. 3 are built in two steps. First, the binary tables (see Sect. 2.2) are fed into the TOPCAT software (Taylor 2005) and the maps are generated using the Plate Carée projection. In those maps, each observation is represented as a point and the median is calculated in cases of overlapping. While the representation of an observation by a point is not as precise as the projection of the real footprint at the surface, a quality result is guaranteed, thanks to the scale of the map and the resolution of the data, as well as their available density (Rousseau & Érard 2019).

The second step consists of the construction of a Hierarchical Progressive Survey (HiPS) with the Hipsgen program of the Centre de Données Astronomiques de Strasbourg (CDS). The HiPS is a multi-resolution data structure (Fernique et al. 2015), based on the Hierarchical Equal Area isoLatitude Pixelization (HEALPix). The HiPS is generated using the TOPCAT maps as inputs and the results are visualized in the Aladin Desktop software[3] (Bonnarel et al. 2000), also developed by the CDS.

The maps of this study are exported from Aladin Desktop in a Mollweide projection. The $I/F_{550\mathrm{nm}}$ and RGB maps (Figs. 2–4) do not benefit from a Framing Camera context map to avoid any misinterpretation. On the contrary, the three spectral slopes maps we present (in Sect. 3, Figs. 5–7) are superimposed to a transparency of 40% on a Framing Camera map. The FC map used as a background is a HiPS reprocessed in Aladin Desktop from a FC clear filter map of Roatsch et al. (2016a) made of data acquired during the Low Altitude Mapping Orbit (LAMO) mission phase (see Fig. B.1). This allows us to benefit from a surface context at high spatial resolution, as provided by the FC. These three maps are also presented in the appendix without the FC context and coordinate grid (Figs. C.1–C.3). The FC LAMO map and the VIR $I/F_{550\mathrm{nm}}$, RGB composites and spectral slope maps are also freely available through the Aladin Desktop software.

We added masks above 75°N and below 60°S on the maps presented in Sect. 3 because of a lack of data and a lower efficiency on the part of the photometric correction in order to avoid any misinterpretation. Finally, features of the Ceres surface which are discussed in the text (craters or remarkable structures) are indicated by the numbers on the maps. These numbers refer to Table 2, which provides the name and the coordinates for each.

3. Global maps of the spectral parameters

3.1. Map of reflectance at 550 nm

Figure 2 represents the map of the reflectance at 550 nm, highlighting its variability across the surface of Ceres. We excluded

[2] The reflectance and the radiance factor are proportional by a factor of π (Hapke 2012).

[3] https://aladin.u-strasbg.fr/AladinDesktop/

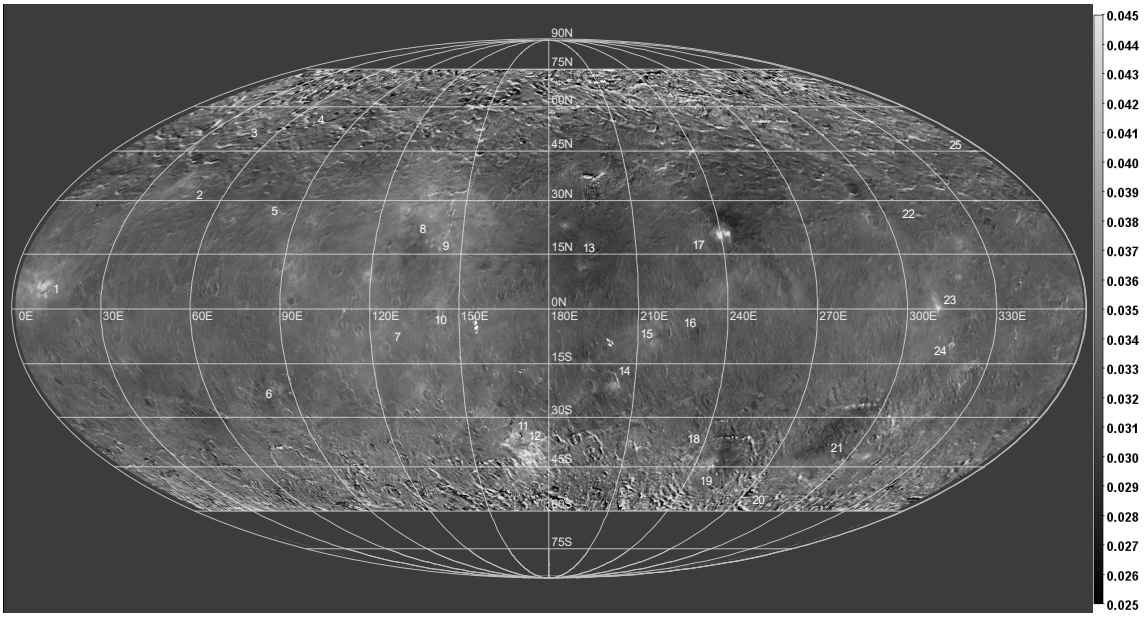

Fig. 2. Map of the VIR reflectance at 550 nm. Numbers refer to the features of Table 2, discussed in the text. White areas correspond to missing data or overexposed spots (e.g., Occator faculae, n°17).

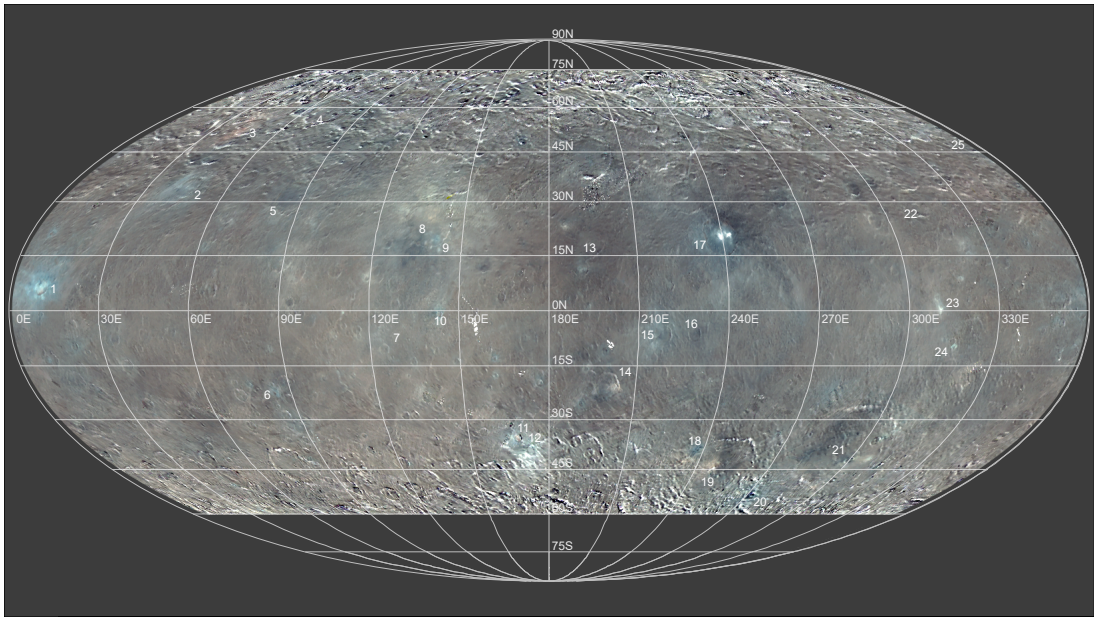

Fig. 3. VIR color composite map made using 950, 550, and 438 nm for the red, green, and blue channels respectively. Numbers refer to the features of Table 2, as discussed in the text. White areas correspond to missing data or overexposed spots (e.g., Occator faculae, n°17).

a total of eight cubes that produced major artifacts. The scale, between 0.025 and 0.045, and the filtering include 94% of the initial 8 million single observations. Some artifacts are still visible in this map and can be of different origins: (1) the effect of the shadows is noticeable at high latitudes, where the photometric correction fails to correct those areas where the geometry of observations is extreme and the signal is very low; (2) possible residuals in the corrections applied to the data (e.g., for the sensor temperature effects, see Sect. 2.2; such kind of artifact is visible as a stripe at, e.g., west of the Braciaca crater); and (3) some small artifacts due to the projection process used to build the maps (e.g. at 195−215°E – 30−35°N).

Nonetheless, we are able to distinguish a certain level of heterogeneities across the surface, which is characterized by median value $I/F_{550\mathrm{nm}}$ of 0.034. This is the case for the center of Vendimia Planitia, which presents an average reflectance of 0.035. Vendimia Planitia owns two major impact craters, Kerwan and Dantu, of which Dantu is easily recognizable because of the contrast in reflectance between the south of the crater and its ejecta which are darker (mean $I/F_{550\mathrm{nm}}$ of 0.034) than the northern part (mean $I/F_{550\mathrm{nm}}$ of 0.037).

Out of Vendimia Planitia, we note different locations with a reflectance that is lower than the average surface. This is the case of the Nawish crater and its ejecta, as well as the internal

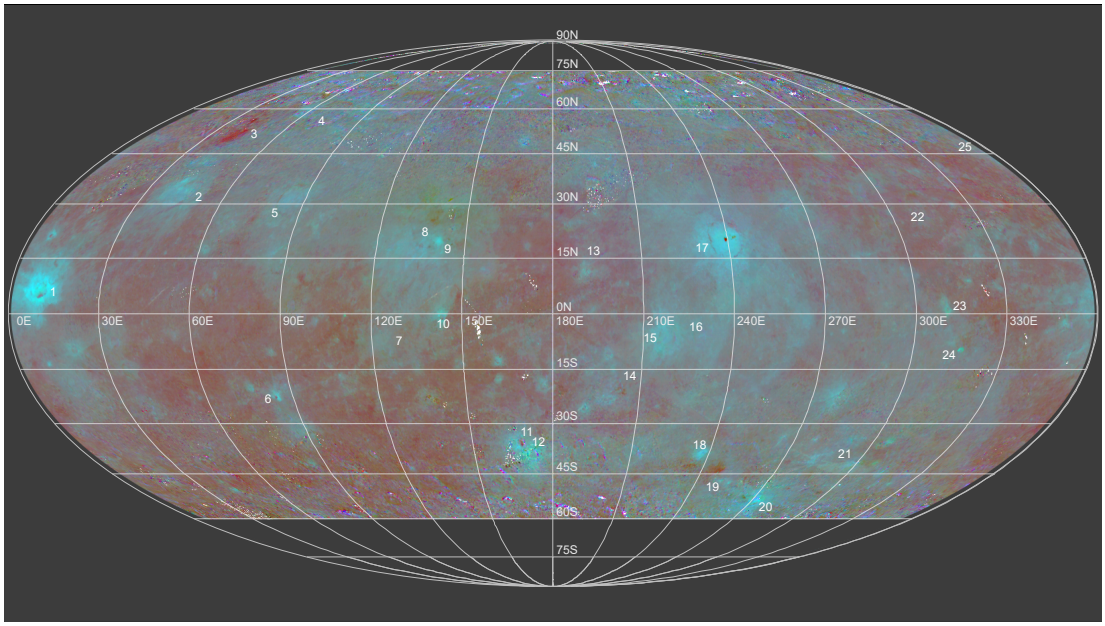

Fig. 4. VIR color composite map made using 950/749, 550/749, and 438/749 ratios for the red, green, and blue channels, respectively. Numbers refer to the features of Table 2, as discussed in the text. White areas correspond to missing data.

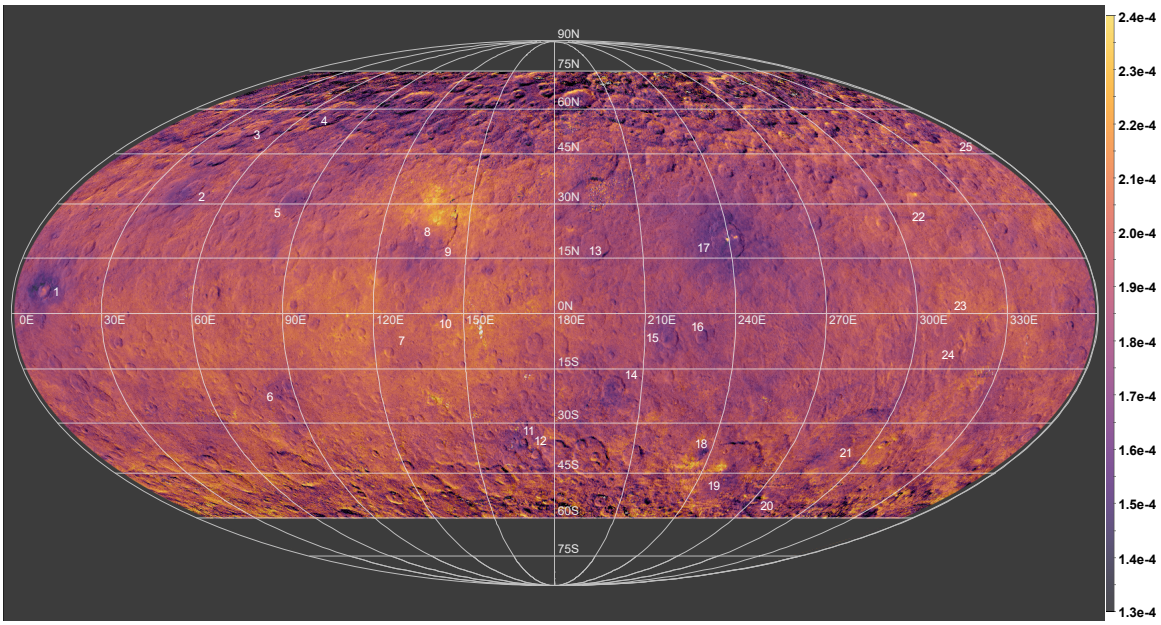

Fig. 5. Map of the VIR $S_{405-465\mathrm{nm}}$ spectral slope superimposed over the FC LAMO map (see Sect. 2.4). Numbers refer to the features of Table 2, as discussed in the text. White areas correspond to missing data.

northeastern and northwestern floors of the Urvara and Yalode craters, and around Occator (for more, see Sect. 4.6).

Ceres is known to have bright spots on its surface, that is, bright material units that stand out with respect to surrounding terrains (Stein et al. 2019). On the reflectance map, the most distinctive bright spots are the two Cerealia and Vinalia faculae within the Occator crater, the young Haulani crater, the region around Kupalo and the Oxo (not visible due to the projection and its location at 0°E; for details on Oxo, see Sect. 4.7) and Xevioso craters. Juling and Kupalo are sufficiently visible in Fig. 2; they actually show high reflectance, but some artifacts, due to the unfavorable observation geometries occurring in those high-latitude areas, are still present around them, particularly to the south of the craters.

3.2. Color composite maps

Figures 3 and 4 are two RGB-color composite maps. The same cubes as for Fig. 2 have been filtered out. Some artifacts are still visible in Fig. 3 (the same as in Fig. 2) but disappear in Fig. 4 due to the use of ratios.

The first color map (Fig. 3) allows the variation of color and reflectance across the surface to be highlighted, providing additional information that is complementary to the $I/F_{550\mathrm{nm}}$ map.